

Adaptive Error Correction for Entanglement Distillation

Sijie Cheng and Narayanan Rengaswamy

Department of Electrical and Computer Engineering, University of Arizona, Tucson AZ 85721
sijiecheng@arizona.edu, narayananr@arizona.edu

Abstract—Quantum network applications impose a variety of requirements on entanglement resources in terms of rate, fidelity, latency, and more. The repeaters in the quantum network must combine good methods for entanglement generation, effective entanglement distillation, and smart routing protocols to satisfy these application requirements. In this work, we focus on quantum error correction-based entanglement distillation in a linear chain of quantum repeaters. While conventional approaches reuse the same distillation scheme over multiple hop lengths after entanglement swaps, we propose a novel adaptive error correction scheme that boosts end-to-end metrics. Specifically, depending on the network operating point, we adapt the code used in distillation over successive rounds to monotonically increase the rate while also improving fidelity. We demonstrate the effectiveness of this strategy using three codes: $[[9, 1, 3]]$, $[[9, 2, 3]]$, $[[9, 3, 3]]$. We compare the performance of four different protocols that combine the codes in different ways, where we define a new performance metric, *efficiency*, that incorporates both overall rate and fidelity. While we highlight our innovation under minimal assumptions on noise, the method can be easily generalized to realistic network settings. By combining our approach with good entanglement generation methods and smart routing protocols, we can achieve application requirements in a systematic, resource-efficient, way.

Index Terms—Quantum repeaters, entanglement distillation, stabilizer code, depolarizing channel, Werner state

I. INTRODUCTION

QUANTUM networks fundamentally differ from classical networks since they rely upon entanglement distribution across the network nodes. Since direct transmission of quantum information across long distances suffers from an exponential scaling of loss [1], quantum repeaters are critical for wide area quantum networks. A repeater generates entanglement across single hops – short links with its neighboring nodes, which could be end-users or other repeaters – and performs entanglement swaps to create longer-range entanglement across longer hops. Since each link introduces loss, and swaps involve local operations that are noisy, *entanglement distillation* is used to distill fewer high fidelity entangled states from many noisy entangled states. Such distillation can be performed on single hops as well as longer hops, as long as classical communication is available across those hops. When end-users place requests for entanglement, the network must

execute a mechanism to deliver entanglement at the necessary rate and fidelity, besides other metrics such as latency. This must be done through a combination of good entanglement generation, efficient distillation and smart routing protocols. Hence, it is essential to develop scalable strategies for these processes that can meet the needs of different applications.

In this paper, we focus specifically on entanglement distillation across single and multiple hops. Entanglement can be distilled using local operations and classical communication (LOCC), which can be one- or two-way [2]. Classic 2-to-1 protocols require the nodes to perform two-way LOCC whereas protocols based on quantum error correction (QEC) only require one-way LOCC, significantly improving efficiency and reducing latency at the cost of increased complexity of LO. We consider QEC-based distillation protocols for second-generation quantum repeaters, where heralded entanglement generation addresses photon loss and QEC is used to correct errors introduced during LO [3]. Since recent years have witnessed an exciting amount of experimental demonstrations of QEC in different hardware technologies [4]–[10], these protocols could indeed be implemented in the next few years. Our goal here is to demonstrate a novel approach to adaptively improve end-to-end metrics that combine both rate and fidelity. Hence, to highlight the key insights and keep the setup simple, we incorporate noise in the channel but assume that all other components are noiseless. We emphasize that our innovation can easily be applied to realistic noise settings.

We consider a linear chain of odd number of repeaters where each repeater generates entanglement with its neighboring nodes, distills, and then swaps them. The process continues until the end nodes have shared Bell pairs that they have distilled themselves. But independent of the length of the chain, we set the maximum number of distillation rounds to 3. The entanglement generation is deterministic but the created state is a *Werner state*, where the Werner parameter could be interpreted as incorporating channel loss as well as noise in LO. These are the minimal assumptions we need to demonstrate our adaptive protocol. Conventional schemes apply the same distillation, or purification, procedure in each round to generate end-to-end entanglement of desired fidelity. However, we start with an $[[n, k, d]]$ stabilizer code, C_1 , with low rate, $R = \frac{k}{n}$, to correct many errors and improve the fidelity after the first round of distillation at single hops. After

This work was supported by the U.S. National Science Foundation under the Engineering Research Centers program, Grant no. 1941583 (“Center for Quantum Networks”).

swapping the resulting k Bell pairs, we adaptively switch to a different $[[n, k' > k, d']]$ code, C_2 , that is able to further improve the fidelity while having a higher rate $R' = \frac{k'}{n} > R$. This is done carefully only when the input fidelity to the first round is just large enough to ensure that the resulting (output) fidelity is above the input fidelity threshold for the second code. For the third round of distillation, we adapt once again by picking yet another $[[n, k'' > k' > k, d''']]$ code, C_3 , if the channel operating point, i.e., depolarizing rate, is suitable. We fix n throughout so that LO need not change greatly.

Our simulations are conducted using the following codes: $C_1 : [[9, 1, 3]]$, $C_2 : [[9, 2, 3]]$, $C_3 : [[9, 3, 3]]$. We compare four protocols: $\mathcal{P}_1 : C_1 - C_1 - C_1$ that uses code C_1 all the time, whereas the other three, $\mathcal{P}_2 : C_1 - C_2 - C_2$, $\mathcal{P}_3 : C_1 - C_2 - C_3$, and $\mathcal{P}_4 : C_2 - C_2 - C_2$, show the regions where they are advantageous. Our metric for comparison is a combination of overall rate (not just the code rate) and fidelity, which we call *efficiency*. Such adaptive QEC for entanglement distillation in quantum repeaters is unprecedented and opens up exciting new ways to achieve end-to-end metrics of quantum network applications. These can be easily modified for more realistic noise settings and the advantages will still qualitatively hold, but for a more sophisticated definition of networking operation point. We leave those deep investigations, especially a general construction of these code sequences as a function of target metrics, the associated fault tolerance requirements, and resource estimates, for future work.

The paper is organized as follows. Section II introduces the necessary technical background, Section III discusses our adaptive protocol, Section IV demonstrates the simulation results for our protocol, and Section V concludes the paper by exploring avenues for future work.

II. BACKGROUND

To better understand the ideas we propose, let us first recall the fundamental concepts and unify the notation used throughout this paper.

A. Stabilizer Formalism

A *stabilizer group*, \mathcal{S} , is a set of commuting Hermitian Pauli operators that does not contain $-I$. The commutativity implies that these operators can be simultaneously diagonalized. Since their eigenvalues are ± 1 , there exist a subspace of quantum states that are $+1$ -eigenvectors of all stabilizers. This subspace is referred to as a *stabilizer code*, $C(\mathcal{S})$. For example, consider a 3-qubit stabilizer group generated by two operators: $S_1 = ZZI, S_2 = IZZ$. A quantum state $|\psi\rangle$ is in the stabilizer code if $S_1|\psi\rangle = |\psi\rangle, S_2|\psi\rangle = |\psi\rangle$. In this case it can be checked that the state takes the form $|\psi\rangle = \alpha|0\rangle + \beta|1\rangle$, where $\alpha, \beta \in \mathbb{C}$ satisfy $|\alpha|^2 + |\beta|^2 = 1$. The logical Pauli operators for the code are those that commute with every stabilizer but do not belong to \mathcal{S} themselves. The weight of a Pauli operator is given by the number of qubits on which it is not the identity, e.g., ZZI has weight 2. If there are $m = n - k$ independent stabilizers on n qubits, and the minimum weight of a logical operator is d , then the code has parameters $[[n, k, d]]$. The above

example gives a $[[3, 1, 1]]$ code since $ZII \equiv IZI \equiv IIZ$ is a logical operator. This formalism simplifies the analysis of quantum error correction and is widely used for code design.

For the purposes of this paper, we will consider the distillation of the standard Bell state $|\Phi^+\rangle = \frac{1}{\sqrt{2}}(|00\rangle + |11\rangle)$. This state forms the one-dimensional $+1$ -eigenspace of the stabilizer group $\mathcal{S}_{++} = \langle +XX, +ZZ \rangle$. The other Bell states $|\Phi^-\rangle = \frac{1}{\sqrt{2}}(|00\rangle - |11\rangle), |\Psi^\pm\rangle = \frac{1}{\sqrt{2}}(|01\rangle \pm |10\rangle)$ correspond to the stabilizer groups $\mathcal{S}_{-+} = \langle -XX, ZZ \rangle, \mathcal{S}_{\pm-} = \langle \pm XX, -ZZ \rangle$. These states can be thought of as the standard Bell state with a Pauli error XI, ZI, YI .

B. Error Syndromes

Errors in a quantum system can be detected using the stabilizer formalism by measuring error syndromes. When an error E acts on a code state $|\psi\rangle$, it may commute or anti-commute with stabilizer operators S_i :

$$E|\psi\rangle = ES_i|\psi\rangle = \pm S_iE|\psi\rangle = \lambda_i S_i(E|\psi\rangle). \quad (1)$$

This means that measuring the stabilizer will give an eigenvalue of $\lambda_i = \pm 1$, where -1 s indicate the presence of an error. The error syndrome is a binary vector that records these eigenvalues: $\mathbf{s} = (\lambda_1, \lambda_2, \dots, \lambda_m)$. For example, consider an error $E = XII$ acting on the $[[3, 1, 1]]$ code defined earlier. We calculate the syndrome as follows:

$$\begin{aligned} ES_1|\psi\rangle &= XII \cdot ZZI|\psi\rangle = -ZZI \cdot XII|\psi\rangle = -S_1E|\psi\rangle, \\ ES_2|\psi\rangle &= XII \cdot IZZ|\psi\rangle = IZZ \cdot XII|\psi\rangle = +S_2E|\psi\rangle. \end{aligned}$$

Thus, the syndrome for this error is: $\mathbf{s} = (-1, +1)$. By measuring the stabilizers, we obtain the syndrome \mathbf{s} , which helps identify which error has occurred. Decoding algorithms use the syndrome to determine and correct the error, restoring the original quantum state if there are not too many errors.

C. Depolarizing Noise Channel

The depolarizing noise channel is a fundamental noise model in quantum information theory. It describes the effect of a qubit undergoing a random Pauli error with a certain probability. For a single-qubit state ρ , it is defined as:

$$\mathcal{E}_p(\rho) = (1 - p)\rho + \frac{p}{3}(X\rho X + Y\rho Y + Z\rho Z), \quad (2)$$

where p is the depolarizing probability. This means that with probability $1 - p$, the qubit remains unchanged, and with probability $\frac{p}{3}$, one of the three Pauli errors X, Y, Z is applied.

In quantum communication, depolarizing noise reduces entanglement fidelity by introducing errors in transmitted qubits. Specifically, when applied to Bell states, depolarizing noise transforms a perfect Bell state $|\Phi^+\rangle$ into a Werner state, a mixed state that retains some entanglement but requires purification for reliable quantum applications.

D. Werner States

A Werner state is a specific type of mixed state obtained when a Bell state is subject to depolarizing noise. Applying the depolarizing channel to $|\Phi^+\rangle$, we obtain:

$$\rho_W = W|\Phi^+\rangle\langle\Phi^+| + (1-W)\frac{I}{4}. \quad (3)$$

Since the identity can be decomposed into Bell states, i.e.,

$$I = |\Phi^+\rangle\langle\Phi^+| + |\Phi^-\rangle\langle\Phi^-| + |\Psi^+\rangle\langle\Psi^+| + |\Psi^-\rangle\langle\Psi^-|, \quad (4)$$

we rewrite ρ_W as:

$$\begin{aligned} \rho_W &= \left(W + \frac{1}{4}(1-W)\right) |\Phi^+\rangle\langle\Phi^+| \\ &+ \frac{1}{4}(1-W) (|\Phi^-\rangle\langle\Phi^-| + |\Psi^+\rangle\langle\Psi^+| + |\Psi^-\rangle\langle\Psi^-|) \\ &= \frac{3W+1}{4} |\Phi^+\rangle\langle\Phi^+| \\ &+ \frac{1}{4}(1-W) (|\Phi^-\rangle\langle\Phi^-| + |\Psi^+\rangle\langle\Psi^+| + |\Psi^-\rangle\langle\Psi^-|). \end{aligned} \quad (5)$$

By defining Fidelity F as $F = \frac{3W+1}{4} \Rightarrow W = \frac{4F-1}{3}$, we express ρ_W in terms of fidelity:

$$\begin{aligned} \rho_W &= F|\Phi^+\rangle\langle\Phi^+| \\ &+ \frac{1-F}{3} (|\Phi^-\rangle\langle\Phi^-| + |\Psi^+\rangle\langle\Psi^+| + |\Psi^-\rangle\langle\Psi^-|). \end{aligned} \quad (6)$$

E. Distillable Entanglement

The efficiency of one-way hashing method is determined by the number of distilled ideal Bell pairs, m , from n pairs of qubits each in a Werner state, given by:

$$D_H = \frac{m}{n} = 1 - S(W), \quad (7)$$

where $S(W)$ is the von Neumann entropy of ρ_W :

$$S(W) = -F \log_2 F - (1-F) \log_2 \left(\frac{1-F}{3}\right). \quad (8)$$

For a Werner state with fidelity F , the distillable entanglement obtained using one-way hashing is [11]:

$$D_H = 1 - S(W) \quad (9)$$

$$= 1 + F \log_2 F + (1-F) \log_2 \left(\frac{1-F}{3}\right). \quad (10)$$

This method is effective when $F > 0.81071$, i.e., $D_H > 0$.

When we have three nodes, let W_1 be the parameter between node 1 and node 2, and W_2 be the parameter between node 2 and node 3. Then, we have the effective Werner parameter

$$\begin{aligned} W_{\text{eff}} &= W_1 W_2 \\ &= \left(\frac{4F_1-1}{3}\right) \left(\frac{4F_2-1}{3}\right), \end{aligned} \quad (11)$$

$$\begin{aligned} F_{\text{eff}} &= \frac{1}{4} + \frac{3}{4} W_{\text{eff}} \\ &= \frac{1}{4} + \frac{3}{4} \left(\frac{4F_1-1}{3}\right) \left(\frac{4F_2-1}{3}\right). \end{aligned} \quad (12)$$

When we have n nodes, we will have W_1, \dots, W_{n+1} , so

$$F_{\text{eff}} = \frac{1}{4} + \frac{3}{4} \prod_{i=1}^{n+1} \left(\frac{4F_i-1}{3}\right). \quad (13)$$

For successful distillation, the threshold condition is:

$$\prod_{i=1}^{n+1} \left(\frac{4F_i-1}{3}\right) > 0.747613. \quad (14)$$

F. Distillation based on Error Correction

The protocol begins with n Bell States shared between Alice and Bob. Instead of sending them directly, Alice projects these states to the subspace of a stabilizer code. Since we use Bell states, the encoding can be implemented via stabilizer measurements on the initial Bell pairs. After encoding, Alice obtains k encoded Bell pairs along with a set of stabilizers. The process is as follows [12], [13]:

- 1) **Encoding:** Alice performs stabilizer measurements on the Bell states to obtain coded Bell pairs.
- 2) **Classical Communication:** Alice sends the stabilizer generators and measurement outcomes (syndromes) to Bob through a classical channel.
- 3) **Noisy Transmission:** Alice transmits one half of the coded Bell pairs to Bob through a noisy quantum channel while keeping the other half.
- 4) **Error Detection:** Upon receiving the transmitted part, Bob applies stabilizer-based syndrome measurements using the same stabilizer generators to detect errors introduced by the channel and obtain the detected syndromes.
- 5) **Error Correction:** Using the stabilizer generators, the syndrome received from Alice, and the detected syndrome, Bob applies decoding to estimate the error and correct it using quantum gates.

If the estimated error matches the actual error, up to stabilizers, then Bob successfully corrects it, restoring the encoded Bell pairs to a perfect state. After successful error correction, Alice and Bob share a set of perfectly encoded Bell pairs, enabling robust long-distance quantum communication.

G. Protocol Rate

In this paper, the protocol rate refers to the ratio of the total number of entanglement links finally established from Alice to Bob and the total number of entangled states consumed throughout the protocol. For a multi-repeater setup, entanglement is generated at each segment of the communication link, potentially distilled, and then swapped. We define:

- n_{in} as the total number of Bell pairs required across all links in the network.
- n_{out} as the final number of successfully shared high-fidelity Bell pairs between Alice and Bob.

Thus, the protocol rate is given by:

$$R = \frac{n_{\text{out}}}{n_{\text{in}}}. \quad (15)$$

A higher protocol rate indicates a more efficient high-fidelity entanglement distribution process.

$[[9, 1, 3]]$	$[[9, 2, 3]]$	$[[9, 3, 3]]$
$H = \begin{bmatrix} YZIIIIIXY \\ ZYZIIIIIX \\ ZZYIIIIIXI \\ IIIIXIIII \\ IIIIXIIII \\ IIIIXIIII \\ IIIIXIIII \\ IIIIXIIII \\ IIIIXIIII \\ IZZIIIIIZZ \end{bmatrix}$	$H = \begin{bmatrix} YZZIIXII \\ ZYZIZIXYY \\ ZIYZIIXYX \\ ZIIXIIIIY \\ IIZYIIXI \\ IIIIXIIII \\ IIIIXIIII \\ ZZZZIIZZZ \end{bmatrix}$	$H = \begin{bmatrix} YZIZIIXYX \\ IXZZIXYIY \\ ZIYZIXIYX \\ IZIYIXXYZ \\ IIIIXIIII \\ IIIIXIIII \\ ZZZZIIZZZ \end{bmatrix}$
$\bar{X} = [ZIIIIIXX]$	$\bar{X} = \begin{bmatrix} IZZIIXXI \\ IZIZIIXIX \end{bmatrix}$	$\bar{X} = \begin{bmatrix} ZIIIXXII \\ IIZZIXIXI \\ IZIZIXIIX \end{bmatrix}$
$\bar{Z} = [ZZIIIIIZ]$	$\bar{Z} = \begin{bmatrix} IZZIZIIZI \\ IZZZIIIZ \end{bmatrix}$	$\bar{Z} = \begin{bmatrix} ZZIZIIZII \\ ZIZZIIZZI \\ ZZZIIZIZ \end{bmatrix}$

TABLE I: The three 9-qubit codes that we use for simulations.

III. ADAPTIVE ERROR CORRECTION PROTOCOL

A. Stabilizer Codes

In this work, we obtain stabilizer codes from the *CodeTables* database [14] and then transform them into standard form as outlined in [15, Chapter 10]. We describe the codes in the form of matrices whose entries are Pauli operators. Each row of the stabilizer matrix H (resp. logical operator matrix \bar{X} or \bar{Z}) corresponds to an independent stabilizer (resp. logical X or logical Z) of the code. To illustrate the main ideas, we focus on the $[[9, 1, 3]]$, $[[9, 2, 3]]$ and $[[9, 3, 3]]$ codes shown in Table I. As an initial test for uncovering structural properties relevant to distillation, we also examine the well-known $[[5, 1, 3]]$ and $[[7, 1, 3]]$ codes. However, we emphasize that our method can be suitably adapted to other sequences of stabilizer codes.

B. Decoder Based on Lookup Table

The lookup table decoder is a method for quantum error correction that maps syndromes to error patterns using a precomputed table. It operates with the following steps:

- 1) **Syndrome Measurement:** The stabilizer measurements yield an error syndrome, $\mathbf{s} = (\lambda_1, \lambda_2, \dots, \lambda_m) \in \{\pm 1\}^m$.
- 2) **Error Identification via Lookup Table:** The syndrome is matched with a stored minimum-weight error in the lookup table as the estimated error. This is the maximum likelihood decoding strategy for the depolarizing channel (i.e., Werner states).
- 3) **Error Correction:** If the estimated error exactly matches the actual error, up to a stabilizer, then decoding is successful. Otherwise, logical operators are used to check which logical qubits are in error.

For $k = 1$ logical qubit, the logical error rate is the same as the per-logical-qubit error rate. However, for $k > 1$ logical qubits, each logical qubit can suffer from different logical error rates. In our results, a lower-bound strategy is used (for output fidelity): the logical error rate for each qubit is taken to be the overall logical error rate of the code. This method provides an efficient way to handle errors in small-distance quantum codes and can be used for practical quantum networking applications.

C. Number of Distillation Rounds

We want to determine a scalable structure for a chain of repeaters based on several rounds of distillation and entanglement swaps to increase the output fidelity.

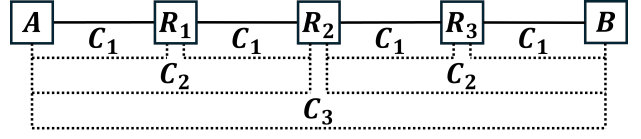


Fig. 1: Protocol diagram for three repeaters.

To determine the optimal number of distillation rounds, the three-repeater situation provides a suitable case for analysis. To clarify, let's start with a three-repeater configuration, with the structure shown in Fig. 1. This setup includes Alice, a chain of repeaters from R1 to R3, and Bob.

First, entanglement links are established between the following adjacent pairs: Alice and R1, R1 and R2, R2 and R3, and R3 and Bob. Next, entanglement distillation is performed independently for each link using code C_1 . Then, quantum swaps are performed to generate entanglement links between Alice and R2, and between R2 and Bob.

Subsequently, distillation is applied using code C_2 between Alice and R2, and between R2 and Bob. In this process, distillation is always performed between the two nodes closest to the current entanglement link. Next, a final quantum swap is performed to establish an entanglement link between Alice and Bob. Finally, end-to-end distillation is carried out between Alice and Bob using code C_3 .

In the first test experiment, we want to start with something simple. So, we use these two codes: $[[5, 1, 3]]$ and $[[7, 1, 3]]$, which are well known for encoding a single logical qubit, but one has a lower rate than the other.

In Fig. 2, the title of each subfigure follows the format "C-X-X", where "C" indicates that distillation is performed in that round, and "X" means that distillation is not performed in the corresponding round. Legends beginning with "OR" indicate cases without repeaters (i.e., these are just logical error rates for the codes). For example:

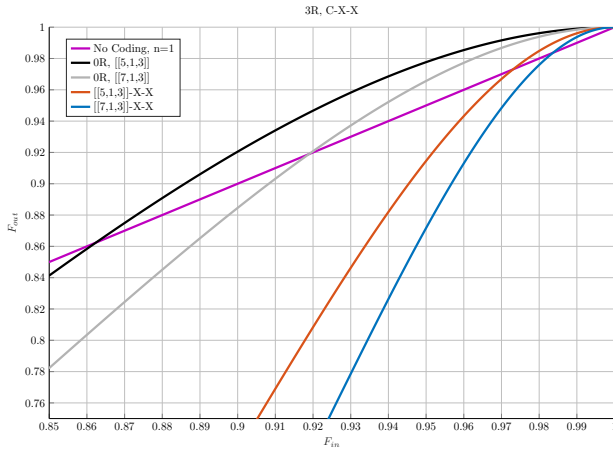
(a) represents performing only the first round of distillation. "OR, $[[5, 1, 3]]$ " and "OR, $[[7, 1, 3]]$ " denote directly establishing the entanglement link between Alice and Bob without repeaters, using the $[[5, 1, 3]]$ and $[[7, 1, 3]]$ codes, respectively. These curves are simply the logical error rates of the codes, plotted as input fidelity vs output fidelity. In this context, " $[[5, 1, 3]]$ -X-X" indicates that only the first round of distillation is performed, using the $[[5, 1, 3]]$ code.

(b) refers to performing the first and second rounds.

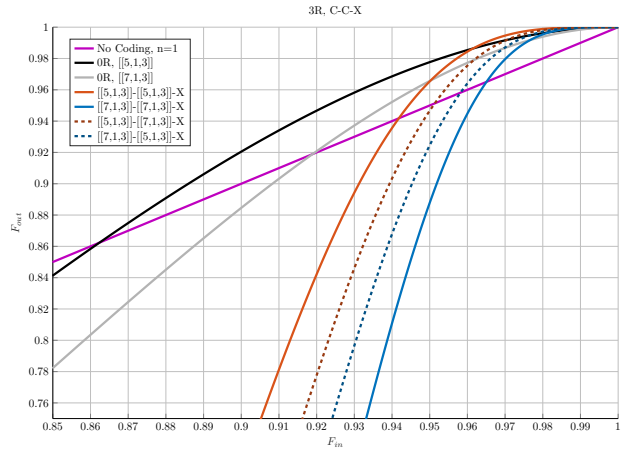
(c) refers to performing the first and third rounds.

(d) refers to performing all three rounds.

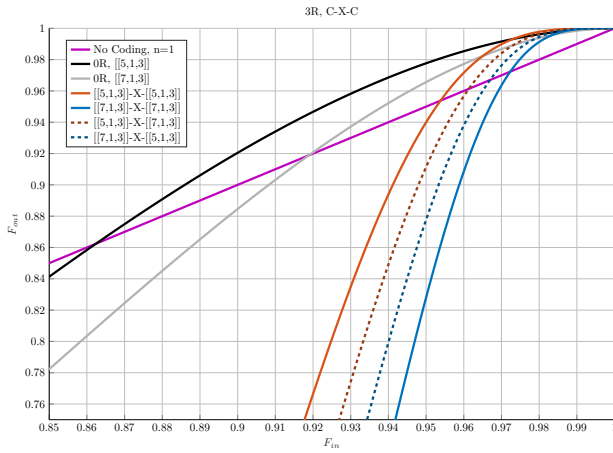
Since, based on our assumption, the depolarizing noise originates from the first round of distillation, the first round is the most important. The final end-to-end round of distillation is also important because it can fix errors generated during intermediate swaps, which makes it the second most important.



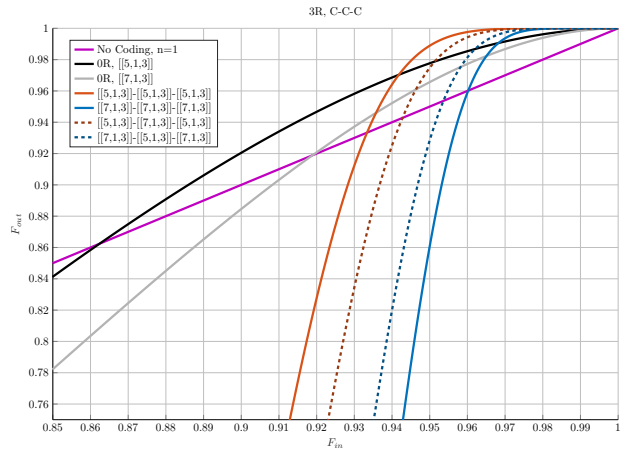
(a) C-X-X



(b) C-C-X



(c) C-X-C



(d) C-C-C

Fig. 2: Three Rounds of Distillation. Legend entry “No Coding” means $F_{\text{out}} = F_{\text{in}}$, that is, no coding is used.

Comparing Fig. 2b and Fig. 2c, both apply the first round, but one includes the second and the other includes the final. As shown in the plots, Fig. 2b performs better, suggesting that having only the first and final rounds may not be enough.

Comparing Fig. 2a, Fig. 2b and Fig. 2d, we find that as the number of rounds increases, the last-performed round in each configuration contributes the least benefit. So the second round ranks third in importance. This suggests that adding more rounds of distillation in the middle provides diminishing benefits as the number of rounds increases, potentially leading to a decrease in the link-building speed. Therefore, it is reasonable to limit the number of distillation rounds to three.

D. Simulation Setup

Given that we fix the number of distillation rounds to three, this strategy can be extended to configurations with any number of repeaters. To clarify, let’s start with a single repeater, with the structure shown in Fig. 3. This means we have Alice, the repeater, and Bob. First, Alice and the repeater, as well as the repeater and Bob, will each generate an entanglement

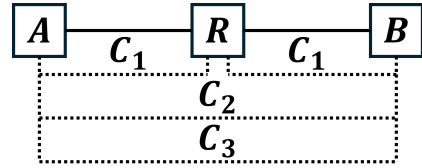


Fig. 3: Protocol diagram for a single repeater, where we still perform three rounds of distillation.

link. Next, they will perform distillation by using code C_1 separately. Then, we will perform a quantum swap to generate the entanglement link between Alice and Bob. Afterward, we will conduct distillation by using code C_2 between Alice and Bob. In this process, we aim to perform distillation between the two nodes that are closest to the current distillation. Finally, an end-to-end distillation by using code C_3 will be performed between Alice and Bob. In this specific situation, we will perform distillation between Alice and Bob twice to align with our three-round distillation strategy.

A more general case is shown in Fig. 4 for the setting of five repeaters, still with three rounds of distillation.

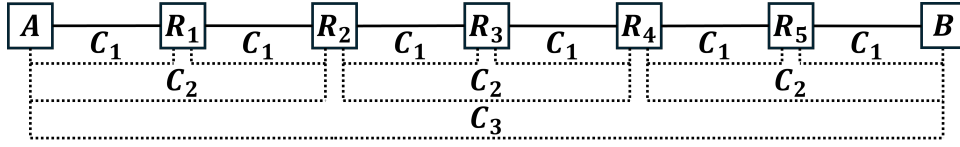


Fig. 4: Protocol diagram for five repeaters, where we perform only three rounds of distillation.

E. Assumptions

For our error correction-based distillation model, we use distillable entanglement as part of the end-to-end metric. To simplify the model, we assume that the only source of noise is the depolarizing channel, while all other components are ideal. This means that whenever we attempt to generate entanglement between two nodes, it will always succeed with 100% probability, and there is no loss in the channel.

We assume that the distance and circumstances between each pair of nodes are identical, meaning they will have the same input fidelity. Therefore, we can use a single input fidelity value to represent the fidelity between all adjacent nodes. Thus, we define this input fidelity as our F_{in} .

The generated Bell pairs are considered ideal, and we simplify the noise model by assuming twirling is applied to produce depolarized Bell pairs. Quantum memories are assumed to hold qubits indefinitely without any decoherence or loss. Additionally, distillation and swapping operations are treated as ideal, with no errors.

These are the minimal assumptions that we need to demonstrate our adaptive error correction protocol. But we emphasize that our methods can be suitably adapted to realistic noise settings, and the advantages will qualitatively hold true.

F. Introduction to the Algorithm

Our simulation setup is built on MATLAB. When we try to build our algorithm, there are two major issues that need to be solved. The first one is the noise generation problem. When generating random Pauli noise, we expect it to be truly random. As is well known, random numbers generated by modern classical computers are all pseudo-random. Thus, generating results that approximate true randomness correctly is a significant goal for our algorithm. The second issue arises from the fact that the final result represents a probability distribution, which means we need a large number of noise simulations to obtain reliable final results. Based on our experiments, each mapping point between input fidelity F_{in} and output fidelity F_{out} requires at least 1,000,000 simulations to obtain a relatively accurate result. As a result, accelerating this process becomes the core goal of the algorithm.

To address these issues, we propose an algorithm which uses a fixed probability to replace random error generation.

1) *Part I: Constructing the Logical Error Rates (OR)*: First, as shown in Fig. 5, we need to construct the F_{in} - F_{out} map for the 0-Repeater case, which will serve as a reference for subsequent parts. When multiple repeaters are introduced, if the input noise is depolarizing, then after performing a quantum swap, the resulting noise remains depolarizing. Therefore,

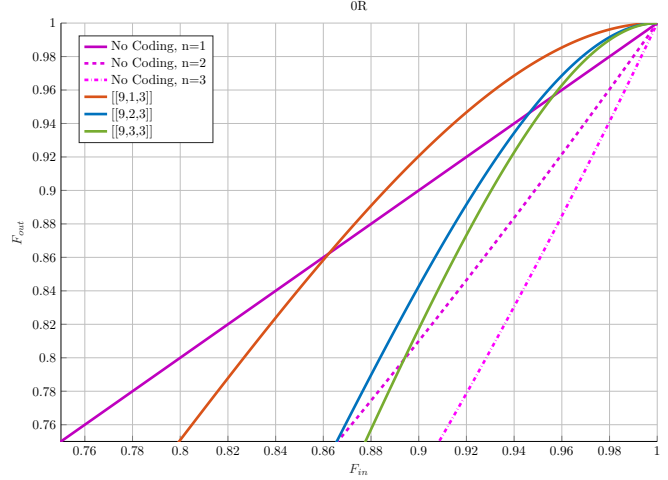


Fig. 5: The F_{in} - F_{out} map for the 0-repeater case. As an example, the plot in the F_{in} - F_{out} map is shown for $[[9, 1, 3]]$, $[[9, 2, 3]]$ and $[[9, 3, 3]]$. Additionally, the no-coding error rates for $n = 1$, $n = 2$ and $n = 3$ are provided as references.

when performing error correction in the next round, we can directly use the F_{in} - F_{out} map from the 0-Repeater case to determine F_{out} after the next round of error correction, thereby accelerating the simulation process.

Step 1: Construct the F_{in} Sequence:

In this step, we uniformly select 1000 points from $F_{in} = 0$ to $F_{out} = 1$. At the same time, we generate the probabilities P_X , P_Y , and P_Z based on the characteristics of depolarizing noise.

Step 2: Construct the All Error List:

We list all possible error events (including the case where no error occurs) and sort them in ascending order based on their error weight. That is, the first error in the list is the most probable error, the second error is the second most probable one, and so on. If we describe the error-correcting code using $[[n, k, d]]$, then the total number of possible error combinations based on the syndrome is $2^{(n-k)}$.

Step 3: Write Data into the All-Error List:

In this step, we need to perform three tasks. Using the points obtained from *Step 1*, calculate the probability of each error combination (for each of the 1000 selected points) and write this into the all-error list. Then, construct the Lookup Table and obtain the logical error based on the logical operator, then write

it into the all-error list.

Step 4: Construct the Lookup Table:

This step is performed simultaneously with *Step 3*. For each processed error combination, we obtain its corresponding syndrome. If this syndrome has not been recorded in the Lookup Table, we record the error combination that triggers this syndrome. If the syndrome has already been recorded, it means that the current error combination is not the smallest-weight error and does not need to be recorded, because in *Step 2*, we have already sorted the errors by weight.

Step 5: Obtain the Logical Error Corresponding to Each Error Combination:

This step is performed simultaneously with *Step 3*. After *Step 4*, we use the logical operator to determine the logical error caused by the current error combination. Then, we retrieve the smallest weight error from the Lookup Table corresponding to this syndrome and test whether it can accurately predict the logical error caused by the current error combination: If it can predict correctly, record it as correctable by the Lookup Table. Otherwise, record it as uncorrectable. Finally, write the results into the error list.

Step 6: Generate the $F_{\text{in}}-F_{\text{out}}$ Map:

From the all-error list, read all correctable logical error probabilities and accumulate them for each of the 1000 points (generated in *Step 1*). In the end, we obtain the $F_{\text{in}}-F_{\text{out}}$ map for 1000 points spanning $F_{\text{in}} = 0$ to $F_{\text{in}} = 1$.

2) *Part II: Constructing the Many-Repeater Situation:*

Before proceeding to this part, we need to repeatedly execute *Part I* to obtain all required $F_{\text{in}}-F_{\text{out}}$ maps for the error-correcting codes being used.

Step 1: Construct the F_{in} sequence:

In this step, we uniformly select a required number of points from $F_{\text{in}} = 0$ to $F_{\text{in}} = 1$ as needed.

Step 2: Perform error correction in this round:

Based on the F_{in} points constructed in *Step 1* and the chosen $[[n, k, d]]$ error-correcting code, we use `interp1()` to look up the corresponding $F_{\text{in}}-F_{\text{out}}$ map in 0-repeater case, where the F_{out} value represents the post-error-correction F_{out} at this round.

Step 3: Compute the output fidelity of entanglement swap:

Based on our discussion in the background (Eqn. (12)), since in this case each round of error correction is based on the same codes, with the same input fidelity at the beginning, we can simplify the formula to the following form:

$F_{\text{eff}} = \frac{1}{4} + \frac{3}{4} \left(\frac{4F_{\text{in}}-1}{3}\right)^{n_{\text{QS}}+1}$, where n_{QS} represents the total number of quantum swaps required in this round. The result obtained from this formula becomes the F_{in} for the next round.

Step 4: Obtain the final $F_{\text{in}}-F_{\text{out}}$ map:

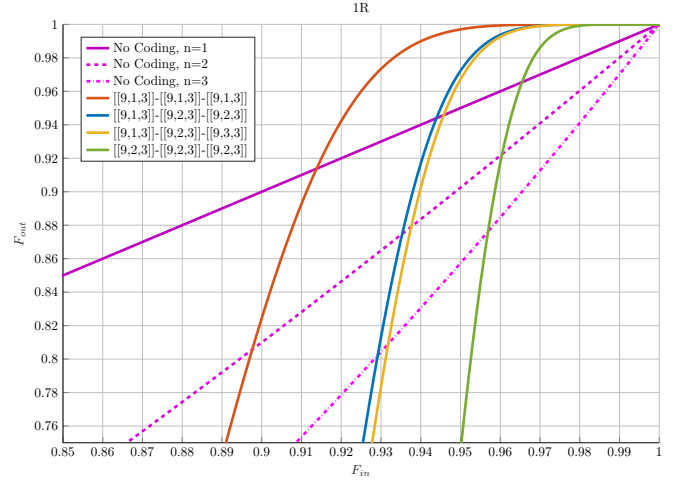


Fig. 6: the $F_{\text{in}}-F_{\text{out}}$ map for the 1-repeater case. This figure only shows the relationship between input fidelity and output fidelity based on different protocols. No coding means that no error-correcting code is used. For example, when $n = 1$, $F_{\text{out}}^{\text{No Coding}} = F_{\text{in}}$, which means that when the input is a single qubit, the output fidelity corresponds to the $n = 1$ qubit case. In general from $F_{\text{out}}^{\text{No Coding}} = F_{\text{in}}^n$.

By repeating *Step 2* and *Step 3* with different codes in each round, we complete error correction across all rounds and obtain the final $F_{\text{in}}-F_{\text{out}}$ map.

IV. SIMULATION RESULTS

A. Goal

Based on the single repeater situation, we can use various coding combinations. To describe this clearly, we will use the notation $[[n_1, k_1, d_1]] - [[n_2, k_2, d_2]] - [[n_3, k_3, d_3]]$ to represent the codes used at each round. For example, $[[9, 1, 3]] - [[9, 2, 3]] - [[9, 3, 3]]$ means we will use $[[9, 1, 3]]$ for the first round. To maintain system stability, we will use the same code for each link within the same round. Then, we will use $[[9, 2, 3]]$ for the second round and $[[9, 3, 3]]$ for the final end-to-end round. Here, we will compare $[[9, 1, 3]] - [[9, 1, 3]] - [[9, 1, 3]]$, $[[9, 1, 3]] - [[9, 2, 3]] - [[9, 2, 3]]$, $[[9, 1, 3]] - [[9, 2, 3]] - [[9, 3, 3]]$ and $[[9, 2, 3]] - [[9, 2, 3]] - [[9, 2, 3]]$.

To simplify our following description, let us define the notation for each protocol:

- Protocol₁: $[[9, 1, 3]] - [[9, 1, 3]] - [[9, 1, 3]]$
- Protocol₂: $[[9, 1, 3]] - [[9, 2, 3]] - [[9, 2, 3]]$
- Protocol₃: $[[9, 1, 3]] - [[9, 2, 3]] - [[9, 3, 3]]$
- Protocol₄: $[[9, 2, 3]] - [[9, 2, 3]] - [[9, 2, 3]]$

Because the number of outputs (i.e., logical qubits) is different across these codes, we will use the fidelity lower bound (see Section III-B) to describe the performance of each. This means that all output qubits being correct simultaneously is considered successful, while any single output qubit failure is considered a total failure. In practice, we wouldn't know which logical qubits are in error, so this is reasonable.

In Fig. 6, we observe that the choice of coding protocol can significantly affect the fidelity. We also observed that the logical qubit rate and distillable entanglement can be affected by different protocols. This implies that it is impossible to achieve an overall optimal result using a single code. Hence, our goal is to develop an adaptive strategy to switch between protocols at relatively optimal thresholds, balancing the trade-off between rate, fidelity, and distillable entanglement.

B. Results

To demonstrate this multi-way tradeoff, we define the *efficiency* function as follows:

$$E(F_{\text{in}}) := \frac{n_{\text{out}}D(F_{\text{out}}(F_{\text{in}}))}{n_{\text{in}}D(F_{\text{in}})} = \frac{R_{\text{out}}D_{\text{out}}(F_{\text{in}})}{D(F_{\text{in}})}, \quad (16)$$

where:

- n_{in} is the number of entangled states consumed,
- n_{out} is the number of output entangled states,
- $R_{\text{out}} = \frac{n_{\text{out}}}{n_{\text{in}}}$ is the protocol rate,
- F_{in} is the input fidelity,
- $F_{\text{out}}(F_{\text{in}})$ is the output fidelity corresponding to F_{in} ,
- $D(F_{\text{in}})$ is the input distillable entanglement,
- $D_{\text{out}}(F_{\text{in}})$ is the output distillable entanglement.

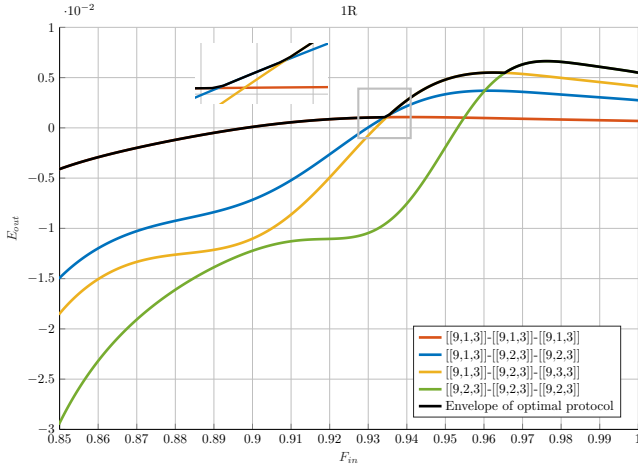
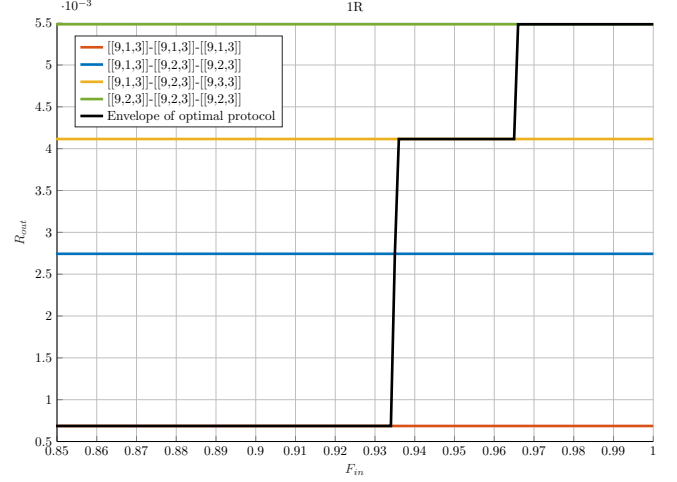


Fig. 7: The $F_{\text{in}}-E_{\text{out}}$ map for the 1-repeater case with the envelope highlighting the optimal protocol. This figure shows the relationship between efficiency and input fidelity, using input fidelity as the reference for adaptive switching. We zoom in on the region where the switch occurs from Protocol₁ to Protocol₃. The reason we include Protocol₂, even though it is optimal only for a very short input fidelity range, is that we aim to minimize changes in k during each round. When switching between two closely spaced adaptive protocols, keeping k as stable as possible ensures smoother system performance, especially when noise varies continuously over time.

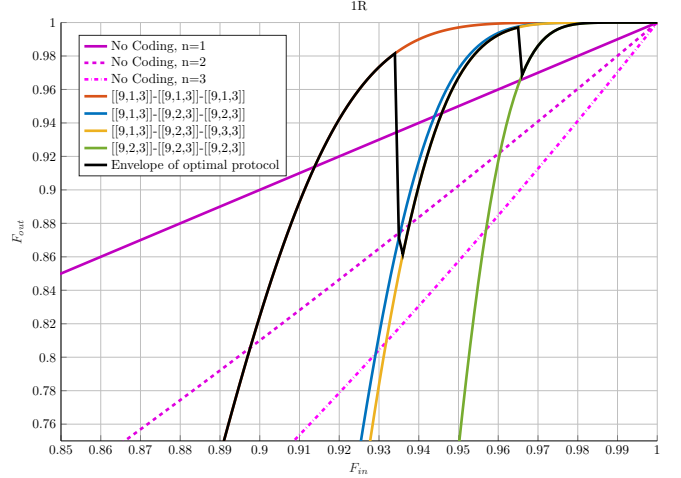
1) *Single Repeater*: Based on our efficiency function, we choose the protocol with the maximum efficiency as the actual protocol to be used, depending on the input fidelity. Finally, we obtain the switching points as follows:

- From Protocol₁ to Protocol₂: $F_{\text{in}} = 0.9343$;
- From Protocol₂ to Protocol₃: $F_{\text{in}} = 0.9356$;
- From Protocol₃ to Protocol₄: $F_{\text{in}} = 0.9655$.

These switching points can be clearly observed in Fig. 7. The corresponding results for $R_{\text{out}}, F_{\text{out}}$ and D_{out} are shown in Figs. 8.a, 8.b and 8.c, respectively.



(8.a) The $F_{\text{in}}-R_{\text{out}}$ map for the 1-repeater case with optimal envelope.

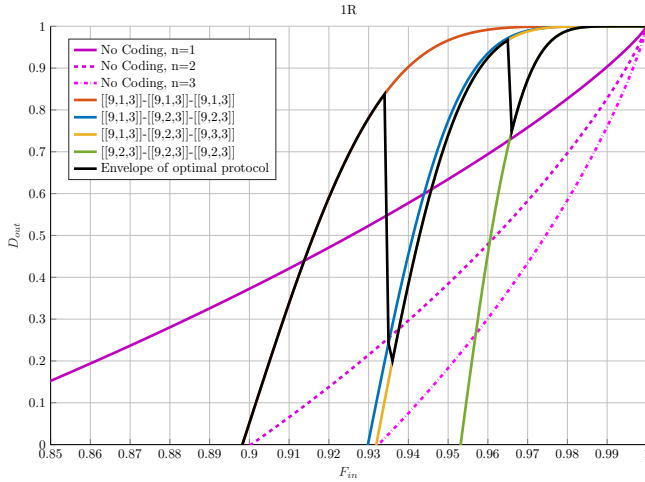


(8.b) The $F_{\text{in}}-F_{\text{out}}$ map for the 1-repeater case with optimal envelope.

2) *Multiple Repeaters*: Based on the discussion in the single-repeater scenario, we found that the critical part is identifying the switching point based on the efficiency function. According to our experiments, we found that for multiple repeaters, they behave similarly to the single-repeater scenario. However, as the number of repeaters increases, all optimal switching points move to the right, meaning that higher input fidelity is required as the trigger to switch between protocols and achieve optimal efficiency.

From Fig. 9, we can identify the switching points for the adaptive protocol on three repeaters as follows:

- From Protocol₁ to Protocol₂: $F_{\text{in}} = 0.9465$;
- From Protocol₂ to Protocol₃: $F_{\text{in}} = 0.9474$;
- From Protocol₃ to Protocol₄: $F_{\text{in}} = 0.9717$.



(8.c) The F_{in} - D_{out} map for the 1-repeater case with optimal envelope.

Fig. 8: The 1-repeater case with optimal envelope. Based on the switching points from the efficiency function, we can observe an increase in the rate in Fig. 8.a as the input fidelity increases. In Fig. 8.b, we can see how the output fidelity changes as the input fidelity increases. In Fig. 8.c, we can see that distillable entanglement follows the same trend as fidelity. The general form of the “No Coding” plots is given by $D_{out}^{No\ Coding} = D_{out}(F_{in}^n)$.

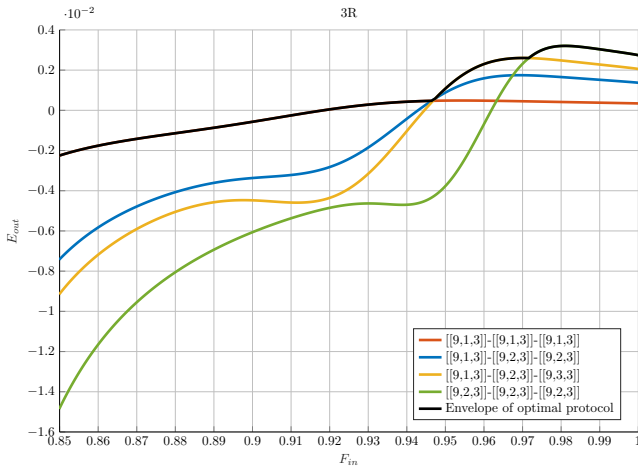


Fig. 9: The F_{in} - E_{out} map for three repeaters with optimal envelope. Observe that the protocol switching points moved to the right compared to the single repeater case.

From Fig. 10, we can identify the switching points for the adaptive protocol on five repeaters as follows:

- From Protocol₁ to Protocol₂: $F_{in} = 0.9524$;
- From Protocol₂ to Protocol₃: $F_{in} = 0.9532$;
- From Protocol₃ to Protocol₄: $F_{in} = 0.9747$.

These have progressively increased from the single repeater

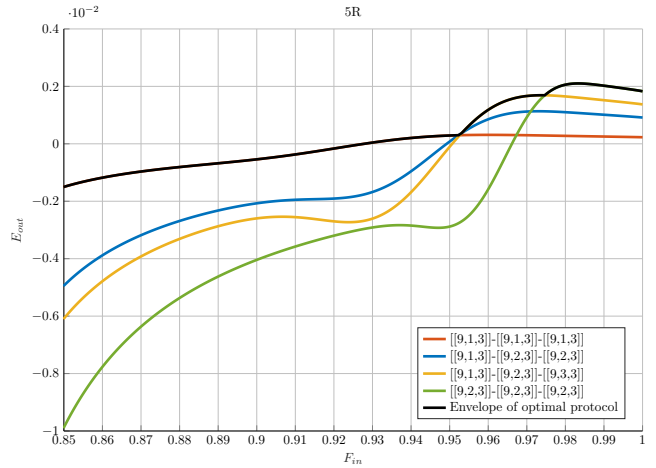


Fig. 10: The F_{in} - E_{out} map for five repeaters with optimal envelope. Observe that the protocol switching points moved to the right compared to the three-repeaters case.

and three repeaters cases. In Table II, we identify the switching points for different numbers of repeaters. We can easily see that the switching point increases with the number of repeaters.

#R	F_{SW}^1	F_{SW}^2	F_{SW}^3
1	0.9343	0.9356	0.9655
3	0.9465	0.9474	0.9717
5	0.9524	0.9532	0.9747
7	0.9561	0.9568	0.9766
9	0.9587	0.9594	0.9780
11	0.9608	0.9614	0.9791
13	0.9624	0.9630	0.9799
101	0.9779	0.9782	0.9881
1001	0.9877	0.9879	0.9934

TABLE II: The relationship between the switching points and the number of repeaters. #R represents the number of repeaters, and F_{SW}^n represents the switching points.

3) *General end-to-end metrics*: Our approach aims to show that by adaptively changing the code used for distillation in each round, we can achieve a higher value for the objective function compared to using a fixed code. We demonstrated this using the efficiency metric $E(F_{in})$. However, our key insight is that as long as the specific metric/objective function depends on both fidelity and rate, the adaptive approach should be advantageous. Even in the presence of realistic noise, an advantage should still be observed when dynamically adjusting the code/protocol depending on the network operating point.

V. CONCLUSION

In this work, we considered a linear chain of repeaters that create entanglement with neighboring repeaters, perform quantum error correction-based entanglement distillation, execute entanglement swaps, and repeat the process until the end nodes have sufficient number of high-fidelity Bell pairs. We introduced a novel adaptive strategy to switch between different codes for each round of distillation, as a function of

the network operating point. Using three 9-qubit codes with increasing rates, we conducted simulations to compare four different protocols that perform three rounds of distillation, independent of the number of repeaters. As our end-to-end metric, we defined a function called the *efficiency*, which depends on the protocol rate as well as input and output distillable entanglement, which in turn depends on the input and output fidelities. We conclusively demonstrated the advantages of the adaptive strategy to maximize the efficiency, where each of the four protocols become optimal for a certain region of input fidelity.

In future work, we will extend this result to realistic noise scenarios and consider fault-tolerant schemes for performing distillation and swaps. Besides, we will combine our protocols with non-error correction-based entanglement purification protocols that have significantly smaller input fidelity thresholds. Then we can begin with such simple protocols, also adaptively switching between different variants, to improve the fidelity until we reach input fidelity thresholds for error correction-based protocols. Such a streamlined strategy will have several practical advantages in real networks. In the past [11], we considered optimal schedules for distillation and swaps at each repeater to maximize end-to-end distillable entanglement. We showed state-of-the-art fidelity thresholds for distilling GHZ states using quantum low-density parity-check (LDPC) codes [13]. We considered such schemes for Bell pair distillation in trapped-ion repeaters [16]. The ultimate goal would be to find the best adaptive strategies as a function of the desired type of entanglement, the hardware technology, the end-to-end metric, and the network topology.

ACKNOWLEDGMENTS

We would like to thank Kaushik Seshadreesan, Filip Rospędek, and Stefan Krastanov for helpful discussions.

REFERENCES

- [1] S. Pirandola, R. Laurenza, C. Ottaviani, and L. Banchi, “Fundamental limits of repeaterless quantum communications,” *Nature Communications*, vol. 8, pp. 1–15, 4 2017.
- [2] C. H. Bennett, D. P. DiVincenzo, J. A. Smolin, and W. K. Wootters, “Mixed-state entanglement and quantum error correction,” *Physical Review A*, vol. 54, pp. 3824–3851, 11 1996.
- [3] “Optimal architectures for long distance quantum communication,” *Scientific Reports*, vol. 6, p. 20463, 2 2016.
- [4] N. Berthussen, J. Dreiling, C. Foltz, J. P. Gaebler, T. M. Gatterman, D. Gresh, N. Hewitt, M. Mills, S. A. Moses, B. Neyenhuis, P. Siegfried, and D. Hayes, “Experiments with the 4d surface code on a qcd quantum computer,” *arXiv:2408.08865*, 8 2024.
- [5] D. Bluvstein, S. J. Evered, A. A. Geim, S. H. Li, H. Zhou, T. Manovitz, S. Ebadi, M. Cain, M. Kalinowski, D. Hangleiter, J. P. B. Ataides, N. Maskara, I. Cong, X. Gao, P. S. Rodriguez, T. Karolyshyn, G. Semeghini, M. J. Gullans, M. Greiner, V. Vuletić, and M. D. Lukin, “Logical quantum processor based on reconfigurable atom arrays,” *Nature*, vol. 626, pp. 58–65, 2 2024.
- [6] M. P. da Silva, C. Ryan-Anderson, J. M. Bello-Rivas, A. Chernoguzov, J. M. Dreiling, C. Foltz, J. P. Gaebler, T. M. Gatterman, D. Hayes, N. Hewitt, J. Johansen, D. Lucchetti, M. Mills, S. A. Moses, B. Neyenhuis, A. Paz, J. Pino, P. Siegfried, J. Strabley, S. J. Wernli, R. P. Stutz, and K. M. Svore, “Demonstration of logical qubits and repeated error correction with better-than-physical error rates,” *arXiv:2404.02280*, 4 2024.

- [7] R. S. Gupta, N. Sundaresan, T. Alexander, C. J. Wood, S. T. Merkel, M. B. Healy, M. Hillenbrand, T. Jochym-O’Connor, J. R. Wootton, T. J. Yoder, A. W. Cross, M. Takita, and B. J. Brown, “Encoding a magic state with beyond break-even fidelity,” *Nature*, vol. 625, pp. 259–263, 1 2024.
- [8] R. Lescanne, M. Villiers, T. Peronin, A. Sarlette, M. Delbecq, B. Huard, T. Kontos, M. Mirrahimi, and Z. Leghtas, “Exponential suppression of bit-flips in a qubit encoded in an oscillator,” *Nature Physics*, vol. 16, pp. 509–513, 3 2020.
- [9] B. W. Reichardt, A. Paetznick, D. Aasen, I. Basov, J. M. Bello-Rivas, P. Bonderson, R. Chao, W. van Dam, M. B. Hastings, A. Paz, M. P. da Silva, A. Sundaram, K. M. Svore, A. Vaschillo, Z. Wang, M. Zanner, W. B. Cairncross, C.-A. Chen, D. Crow, H. Kim, J. M. Kindem, J. King, M. McDonald, M. A. Norcia, A. Ryou, M. Stone, L. Wadleigh, K. Barnes, P. Battaglini, T. C. Bohdanowicz, G. Booth, A. Brown, M. O. Brown, K. Cassella, R. Cox, J. M. Epstein, M. Feldkamp, C. Griger, E. Halperin, A. Heinz, F. Hummel, M. Jaffe, A. M. W. Jones, E. Kapit, K. Kotru, J. Lauigan, M. Li, J. Marjanovic, E. Megidish, M. Meredith, R. Morshead, J. A. Muniz, S. Narayanaswami, C. Nishiguchi, T. Paule, K. A. Pawlak, K. L. Pudenz, D. R. Pérez, J. Simon, A. Smull, D. Stack, M. Urbaneck, R. J. M. van de Veurdonk, Z. Vendeiro, R. T. Weverka, T. Wilkason, T.-Y. Wu, X. Xie, E. Zaly-Geller, X. Zhang, and B. J. Bloom, “Logical computation demonstrated with a neutral atom quantum processor,” *arXiv:2411.11822*, 11 2024.
- [10] P. S. Rodriguez, J. M. Robinson, P. N. Jepsen, Z. He, C. Duckering, C. Zhao, K.-H. Wu, J. Campo, K. Bagnall, M. Kwon, T. Karolyshyn, P. Weinberg, M. Cain, S. J. Evered, A. A. Geim, M. Kalinowski, S. H. Li, T. Manovitz, J. Amato-Grill, J. I. Basham, L. Bernstein, B. Braverman, A. Bylinskii, A. Choukri, R. Deangelo, F. Fang, C. Fieweger, P. Frederick, D. Haines, M. Hamdan, J. Hammett, N. Hsu, M.-G. Hu, F. Huber, N. Jia, D. Kedar, M. Kornjača, F. Liu, J. Long, J. Lopatin, P. L. S. Lopes, X.-Z. Luo, T. M. Macrì, O. M. Marković, L. A. Martínez-Martínez, X. Meng, S. Ostermann, E. Ostroumov, D. Paquette, Z. Qiang, V. Shofman, A. Singh, M. Singh, N. Sinha, H. Thoreen, N. Wan, Y. Wang, D. Waxman-Lenz, T. Wong, J. Wurtz, A. Zhdanov, L. Zheng, M. Greiner, A. Keesling, N. Gemelke, V. V. Vuletić, T. Kitagawa, S.-T. Wang, D. Bluvstein, M. D. Lukin, A. Lukin, H. Zhou, and S. H. Cantú, “Experimental demonstration of logical magic state distillation,” *arXiv:2412.15165*, 12 2024.
- [11] A. Patil, M. Pacenti, B. Vasić, S. Guha, and N. Rengaswamy, “Entanglement Routing using Quantum Error Correction for Distillation,” *arXiv preprint*, May 2024.
- [12] M. M. Wilde, H. Krovi, and T. A. Brun, “Convolutional entanglement distillation,” in *IEEE International Symposium on Information Theory*, pp. 2657–2661, 8 2010.
- [13] N. Rengaswamy, N. Raveendran, A. Raina, and B. Vasić, “Entanglement purification with quantum LDPC codes and iterative decoding,” *Quantum*, vol. 8, p. 1233, 1 2024.
- [14] M. Grassl, “Bounds on the minimum distance of linear codes and quantum codes.” Online available at <http://www.codetables.de>, 2007.
- [15] M. A. Nielsen and I. L. Chuang, *Quantum Computation and Quantum Information: 10th Anniversary Edition*. Cambridge University Press, 10th anniversary edition ed., 2010.
- [16] A. Kang, S. Guha, N. Rengaswamy, and K. P. Seshadreesan, “Trapped ion quantum repeaters with entanglement distillation based on quantum LDPC codes,” in *IEEE International Conference on Quantum Computing and Engineering (QCE)*, vol. 1, pp. 1165–1171, Institute of Electrical and Electronics Engineers Inc., 2023.